Journal of Power Sources 227 (2013) 137–144

Contents lists available at SciVerse ScienceDirect

Journal of Power Sources

journal homepage: www.elsevier.com/locate/jpowsour

Decreasing contact resistance in proton-exchange membrane fuel cells with metal bipolar plates

Christopher J. Netwall, Benjamin D. Gould, Joseph A. Rodgers, Nicholas J. Nasello, Karen E. Swider-Lyons*

US Naval Research Laboratory, Washington, DC 20375, USA

HIGHLIGHTS

- A PEMFC with metal bipolar plates and state-of-the-art materials is optimized for low resistance.
- A compression break-in cycle and then subsequent compression at >1.00 MPa lowers the resistance.
- The bipolar-plate surface roughness affects the resistive contact with the gas diffusion layers.
- Contact resistance dominates the I^2R losses in a state-of-the-art PEMFC stack.

ARTICLE INFO

Article history:
Received 5 September 2012
Received in revised form
25 October 2012
Accepted 2 November 2012
Available online 17 November 2012

Keywords:
Fuel cell
Contact resistance
Clamping pressure
Metal bipolar-plate

ABSTRACT

Ohmic, or I^2R, losses occur in electrochemical devices, such as proton -exchange membrane fuel cells (PEMFCs) due to the resistance of materials and the contact resistance between the electrochemical active area, the gas diffusion and current collector materials. Such losses must be lessened to maximize the conversion of chemical energy to electricity rather than heat. We probe how to decrease the contact resistance in PEMFCs with metal bipolar plates with state-of-the-art membrane electrode assemblies, specifically Au/TiO_2-coated titanium bipolar plates (BPPs), gas diffusion layers with microporous layers (GDLs with MPLs), and catalyst-coated membranes (CCMs) comprising a 15-μm-thick proton-exchange membranes. Through *in situ* tests of a model system, we find that the system resistance decreases after a compression break-in cycle and then remains low subsequently by keeping the stack assembly compressed at >1 MPa. *Ex situ* tests show that the surface roughness of the BPPs also affects contact resistance with the GDLs. After accounting for the bulk resistance of the cell constituents (BPPs, GDLs, MPLs and CCMs), we conclude that in a state-of-the-art PEMFC, the contact resistances between the materials contribute 55% of the total I^2R losses, and thus dominate the ohmic loss contributions.

Published by Elsevier B.V.

1. Introduction

Proton-exchange membrane fuel cells (PEMFCs) are approximately 50% efficient at the conversion of hydrogen fuel chemical potential to electrical energy, with the remainder of the hydrogen energy converted to heat through activation, mass transport and ohmic, or I^2R losses, the latter which are caused by materials and interfacial resistances [1]. The activation losses are mainly due to the inefficiencies of the cathode catalyst for the oxygen reduction reaction. The mass transport losses occur primarily at the cathode under high power operation, and are derived from the gradient needed to transport O_2 gas through the N_2 and water present in the porous electrodes found in fuel cells. At low current densities, kinetic losses dominate, while mass transport losses are the largest contributor at high current densities.

Also increasing with current density are ohmic, or I^2R, losses in fuel cells, which have long been dominated by the ionic resistance of the proton-exchange membrane (PEM), typically perfluorosulfonic acid (PFSA). The PEM resistance has decreased as manufacturing improvements have led to the development of thinner PEMs, thus decreasing the membrane geometric area over thickness [2,3]. With state-of-the-art PEMs, a significant contributor to the ohmic losses in PEMFCs is from the interfacial contact resistance between the materials in the fuel cell, such as the BPPs and the materials in the MEA, i.e., gas diffusion layers with microporous layers (GDLs with MPLs) and catalyst-coated membranes (CCMs) which comprise the PEM and its catalyst layer.

Another significant change in PEMFC technology has been the movement from carbon BPPs to metal ones. The BPPs have a range of functions, including heat, current and gas flow. The carbon BPPs, originally developed for phosphoric acid fuel cells, are expensive and fragile under compression stresses because of their relatively low flexural strength (20–95 MPa) [4], and any resulting cracks

* Corresponding author. Tel.: +1 202 404 3314; fax: +1 202 404 8119.
E-mail address: karen.lyons@nrl.navy.mil (K.E. Swider-Lyons).

0378-7753/$ – see front matter Published by Elsevier B.V.
http://dx.doi.org/10.1016/j.jpowsour.2012.11.012

result in coolant and gas leakage. Metal plates are becoming the standard for PEMFC BPPs as they have been identified as a path to low-cost, compact fuel cell stacks, especially now that it is well understood how to stop membrane degradation in the presence of trace metals from metal corrosion via the addition of Mn and/or Ce ions [5]. Metal BPPs can sustain larger stress than the carbon BPPs, permitting a larger range of compression, test and operational conditions. Metal BPPs, particularly those made from stainless steel (e.g., 316L), can exhibit increased interfacial contact resistance over carbon BPPs because of oxide scale formation and inherent asperities that reduce contact area [6–10]. Numerous studies have been made on how to lower contact resistance on metal BPPs [6].

While most industrial metal BPPs are made from 316L stainless steel, we use titanium alloys to make prototype BPPs, because titanium provides a high strength and low weight substructure ideal for aerospace applications. The prototype titanium-alloy BPPs are made by a laser-forming-based rapid manufacturing method, direct metal laser sintering (DMLS). An overview of laser methods for rapid manufacturing is given by Santos et al. [11]. DMLS permits the complex design of miniature flow fields and internal cooling channels not available with standard machining processes, and avoids the need for expensive tooling [12]. To minimize their surface resistance and improve their corrosion resistance in the corrosive PEMFC environment, these BPPs are coated with a low-cost, robust, conductive TiO_2/gold coating, which was originally developed to coat stainless steel bipolar plates [13]. In this conductive coating, Au microdots are dispersed throughout the ceramic coating, resulting in a low resistance of 10 mΩ cm^2 with only a 2.4% coating of gold.

The interfacial contact resistance in PEMFCs is also highly dependent on the force used to clamp together the stack components [14], so we combine a mechanical press with a fuel cell test station to minimize cell resistance vs. compression. Standard analytical fuel cell test cells are not configured for measuring performance under variable compressive load. Usually, a compressive load is applied to the circumferential bolts of test cells using a torque wrench, as in our previous works [15]. A steady mechanical load is used here as an accurate representation of the actual force applied to a test cell.

We also probe different surface topologies of BPP, as this is known to affect their contact resistance with the porous gas diffusion layers contact [16,17]. Another factor, which affects interfacial resistance, is the flow field structure, as it can affect the contact stress distribution [18]; we do not optimize for this parameter and instead use a fixed parallel flow field.

By combining high quality components (metal BPPs, GDLs, CCMs) and carrying out realistic tests both *in situ* and *ex situ* using a controlled external mechanical press, the source of materials losses is quantified for a state-of-the-art PEMFC assembly. The research also leads to general procedures for the assembly of high performance fuel cell assemblies including mechanical break-in procedures, and a path to high quality test cells.

2. Experimental

2.1. Materials

Custom BPPs were made from Titanium T64 alloy by DMLS by 3T RPD Ltd (Berkshire, UK). After fabrication, the plates were etched in acid to remove any soluble transition metal impurities (V, Fe) and then coated with a layer of TiO_2 and gold microdots by Treadstone Inc. (Princeton NJ).

The BPP flow field was a typical parallel flow design with flow features for an electrode active area of 22 cm^2. The planar view of the flow field is shown in Fig. 1. The three relevant areas that are used in calculations throughout this work are shaded in the figure. The solid line outlined area shows the geometric electrode area. This value is used for normalizing all resistance measurements to an area-specific resistance common to fuel cells literature. The blue highlighted area shows the land area used to determine the land stress, which is commonly reported in contact resistance literature [20–22]. The dashed line area shows the total force area used to determine the equivalent distributed stress on the cell. The distributed stress is a departure from previous contact resistance works that only examined BPP or flat material samples. The use of an equivalent distributed stress is needed to account for the stress carried by gasket area in operating fuel cells.

Three BPP surface finishes were evaluated for contact resistance to give a broad range of finishes: (1) DMLS finish – the surface finish left after the manufacturing process; (2) Hand polished finish – achieved by wet sanding with 600-grit SiC paper on a granite surface plate; and (3) MicroTek polished finish – a commercial but proprietary process that involves mechanical-catalytic surface activation [23], and is ideal for polishing surfaces with complex geometries. The surface characteristics of each finish, including the arithmetic average roughness (Sa), were characterized using a STIL profilometer with a CL2 lens and M70 magnifier. In this configuration the profilometer had a 300-μm range, a 0.012-μm axial resolution and a 52-μm spot size. Multiple areas of 1 mm × 5 mm were probed on the BPP to acquire represented surface scans.

The GDLs in every experiment comprised 25 BC GDLs (SGL Group), which contain a microporous layer (MPL) on one side and are ideal for high power fuel cell applications. The MPL is important for maximizing fuel cell performance, but makes contact resistance measurements more difficult because the GDL is not symmetric.

Primea-series catalyst-coated membranes (CMMs, W.L. Gore) were used with platinum loadings of 0.1 mg Pt cm^{-2} on the anode and 0.4 mg Pt cm^{-2} on the cathode separated by a 15-μm-thick PFSA supported membrane.

2.2. In situ testing

Prior to *in situ* resistance testing, all MEAs went through a standard fuel cell break-in procedure of cycling between cell voltages to hydrate the membrane and activate the electrode [15]. *In situ* resistance testing was performed on an operating fuel cell at

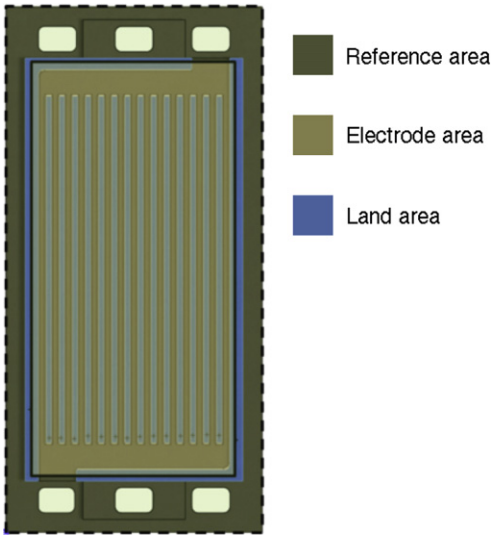

Fig. 1. Planar view of 22 cm^2 BPP detailing the three important areas for contact resistance and applied stress, reference area over the entire plate, 22 cm^2 electrode area, and raised land area.

96% RH and at 0.85 A cm^{-2}. The influence of compressive stress was studied first followed by a sweep of cell temperature after a suitable compression was determined. The total ohmic resistance of the fuel cell was measured by current interrupt and by high frequency impedance using a Scribner 580e Test Station with built-in frequency generator. Both methods yielded consistent resistance measurements. The resistance measurements were taken over a period of several minutes, while the resistance settled to a stable value. The average resistance measurement over the last 1 min of stable measurement was recorded prior to proceeding to the next measurement.

The fuel cell setup had to be modified from previous work to accommodate one piece BPPs [15]. This is different from the machined flow fields in typical analytical fuel cells, which capture half the features of a BPP. The fuel cell test fixture is a modified Fuel Cell Technologies 25 cm^2 test fixture. A cross sectional view of the *in situ* setup detailing all the layers and individual cell components is depicted in Fig. 2. Unlike the majority of single-cell test fixtures, this single-cell requires 2 additional GDLs to make contact with the current collectors from the sides of the BPP not contacting the CCM. A pocketed graphitic carbon end plate (Gr) was used to conduct current and manifold gases to the anode/cathode. MicroTek polished BPPs were used in the *in situ* tests. 150-μm-thick Teflon coated fiberglass picture frames were used to set the GDL pinch and keep the carbon end plates from shorting. The gasketing material for sealing the cell was 1.7-mm-thick fluorosilicone rubber sheet from Stockwell elastomerics, Inc.

The compression force applied to the fuel cell was controlled using a Chatillon LR 50k mechanical press. The press applies a known force from which stress was calculated for the relevant areas. Insulating G10 spacers were used to electronically isolate the press from the load cell. Initially, the cell was compressed to 1.00 ± 0.06 MPa (145 ± 8 psi) at 80 °C and relaxed to 0.14 MPa (100 psi) to perform mechanical break-in prior to resistance measurements as a function of increasing compression stress.

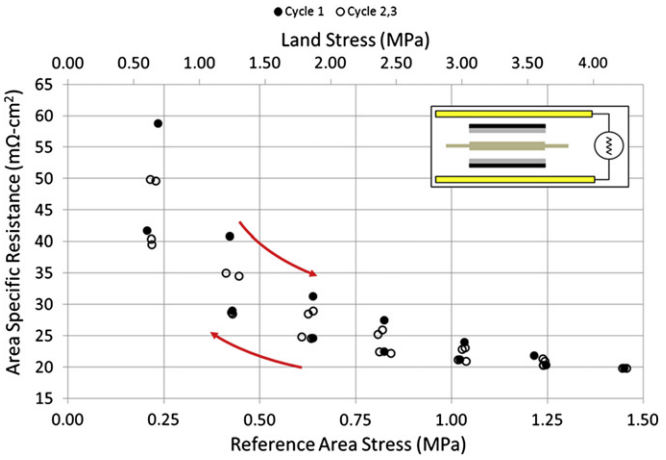

Fig. 3. Compressive cycling showing mechanical break-in. (inset) Schematic of simplified test cell with GDL and BPP, based on Fig. 2. *Ex situ* test at ambient conditions.

Following the compression sweep the cell's compression stress was set to 1.00 MPa (145 psi) at 80 °C and the cell's temperature was varied. After testing the cell was disassembled and GDLs were examined for excessive wear or extrusion into the flow fields.

2.3. Ex situ testing

The through-plane resistances of fuel cell components and assemblies of fuel cell components were measured *ex situ* (i.e., not in an operational fuel cell) to determine the contribution of individual components to the total resistance observed during *in situ* testing. The *ex situ* resistances were measured using a Keithley 580 micro-ohmmeter as the load was incrementally increased from 0.00 MPa to a maximum of 1.72 MPa (250 psi) using the previously described mechanical press. This approach is similar to the work by

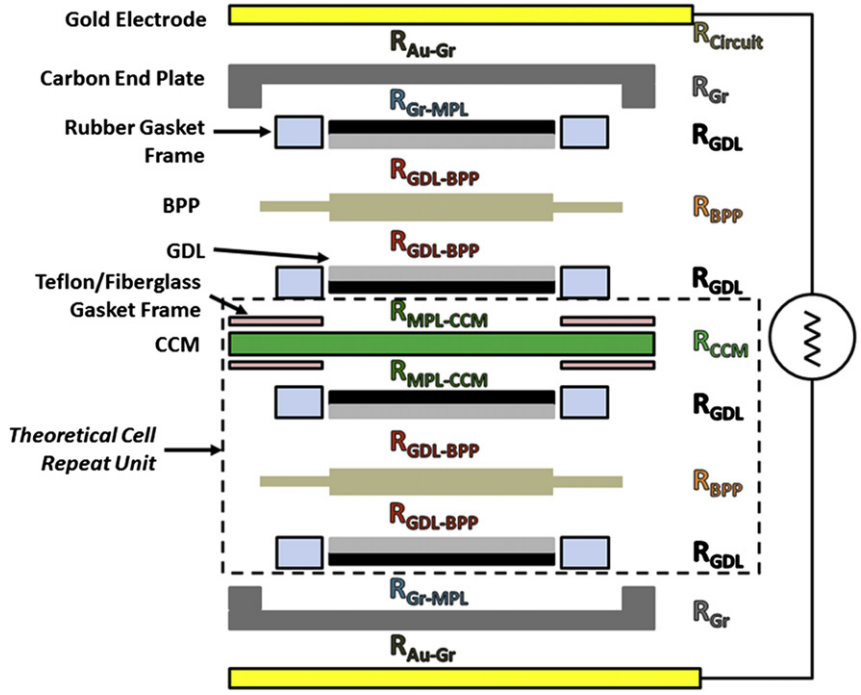

Fig. 2. Cross sectional view of 22 cm^2 *in situ* test configuration defining cell components and resistive components. Parts of this test configuration are used for the *ex situ* testing cells. Legend: Au = gold current collector electrode; Gr = graphitic carbon end plate; BPP = bipolar-plate; GDL = gas diffusion layer; MPL = microporous layer; CCM = catalyst-coated membrane.

Hu's group [24]. The micro-ohmmeter has a resolution of 10 μΩ, which provides 2 digits of resolution greater than was needed for the observed resistances. Three compression cycles were run for each test configuration. The reported values are the average of the three compression cycles taken at 1.00 ± 0.06 MPa (145 ± 8 psi). Plate to plate variability was not examined in this work. The zero stress data point was tested and recorded to complete the stress cycle, but not analyzed because it did not qualitatively add to the observed trend and is an invalid operating condition for a fuel cell.

2.4. Contact resistance analysis

Interfacial contact resistance cannot be observed directly because it is convoluted with materials resistances and other interfacial resistances, if significant. A well-known approach to determining interfacial contact resistance is to use multiple test configurations with variations of the materials and contact interfaces from which the contact resistance can be devolved [17]. In an operating fuel cell there are numerous resistances that contribute to the observed ohmic resistance. The total cell resistance is comprised of 5 unique bulk resistances and 4 unique interfacial contact resistances. As shown in Fig. 2, the bulk resistances arise from the circuit and gold (Au) current collector electrodes, graphitic carbon end plate (Gr) in the test cell, GDL (with MPL), BPP, and CCM. The interfacial resistances are due to the contact between the GDL and BPP, MPL and CCM, Gr and MPL and Au current collector and Gr.

The GDL to BPP interfacial contact resistance ($R_{GDL-BPP}$) is determined using Eqns. (1)–(3). The total resistance of set-up1 (R_{tot1}) and set-up2 (R_{tot2}) is based on the set-ups described in the work by Haldar's group [17].

$$R_{tot1} = 2{*}R_{Au-MPL} + 2{*}R_{BPP-GDL} + 2{*}R_{GDL} + 2{*}R_{BPP} + R_{circuit} \quad (1)$$

$$R_{tot2} = R_{Au-MPL} + R_{Au-GDL} + R_{GDL} + R_{circuit} \quad (2)$$

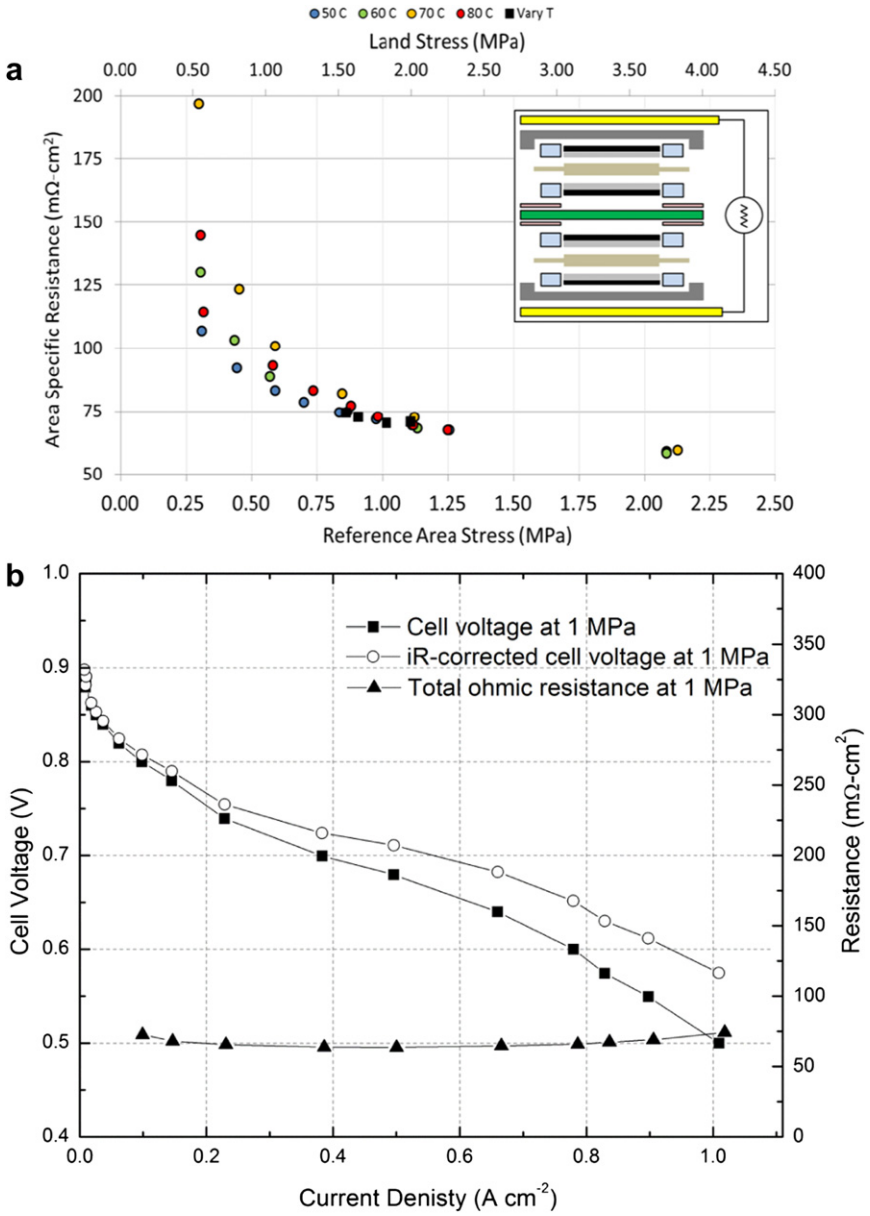

Fig. 4. (a) *In situ* resistance measurements 0.85 A cm^{-2} and at various temperatures and stresses; (a, inset) test cell configuration based on Fig. 2. (b) Polarization curve measured from the cell configuration at 1.00 MPa, 100% RH, 2|2 H^2|air stoichiometry, 80 °C, and ambient pressure.

$$R_{BPP-GDL} = \frac{1}{2}*\left\{R_{tot1} + 2*\left[\frac{1}{2}*(R_{tot2} - R_{GDL} - R_{circuit})\right] - 2*R_{GDL} - R_{BPP} - R_{circuit}\right\} = \frac{1}{2}*(R_{tot1} - R_{tot2} - R_{GDL} - R_{BPP}) \quad (3)$$

Two approximations are used in the analysis. First, it is assumed that the contact resistance at the Au electrode to the MPL of the GDL is the same as the Au electrode to the GDL without a microporous layer ($2R_{Au-MPL} = R_{Au-MPL} + R_{Au-GDL}$). Second, the bulk resistance for the GDL is based on a similar material in the literature, but not SGL 25BC [25]. Both materials are fibrous carbon papers of similar thickness and porosity, so the assumption seems to be valid. Similar mathematical treatments were used for our other test configurations.

3. Results and discussion

The first step was to determine the optimal compressive load for these experiments. Fig. 3 shows a series of three compression/decompression cycles up to 1.4 MPa for an *ex situ* fuel cell assembly comprising a BPP with GDLs on each side. The first compression cycle exhibits hysteresis in the through-plane resistance as a function of compression stress indicative of a mechanical "break-in" response. Subsequent decompression and compression/decompression cycles all follow the same path. This initial break-in is attributed to the GDL being formed into compression with the BPP, as evidenced by observed deformation of the GDL after the cell disassembly. Similar resistance trends with cyclic compression have been observed in recent work [26]. After the first break-in cycle, the cell resistance vs. stress is constant and follows an asymptotic trend. The resistance is near its minimum at a compressive load of >1 MPa for the reference area of the BPP, as has been reported by others [14,18].

To quantify the optimal reference area load, a complete single-cell was assembled and tested for ohmic resistance at different compressive loads and different operating temperatures. It also provides a meaningful complement to the *ex situ* data. Note that since the metal BPPs are one piece, two BPPs must be used to form one cell and provide extra resistance not typically encountered in standardized experiments [15]. The results of this test in Fig. 4a show the effects of temperature on resistance through an operational fuel cell. The circles represent constant temperature tests with varying load; the squares represent a varying temperature test where the load was set to 1.00 MPa (145 psi) at 80 °C and allowed to change with temperature.

Resistance converges to a temperature independent value at stresses above 1.00 MPa (145 psi). It continues to decrease with increasing stress, but inspection of the GDL after the 2.07 MPa (300 psi) test point revealed significant material damage. The improvement in performance at stresses greater than 1.38 MPa (200 psi) is negligible compared to the risk of over-compression of the GDLs, which would inhibit mass transport [14].

Representative polarization curves are shown in Fig. 4b, confirming the function of our custom fuel cell test assembly in Fig. 2. The uncorrected polarization curve is relatively low because of the additional interfaces present in our test cell. Nonetheless, the polarization curve is far superior to what has been reported in other *in situ* compression cells [19], presumably due to the use of all state-of-the-art components and a viable flow field configuration. The *iR*-corrected polarization curve shows that the polarization curve at high current density is below what is measured in our typical single-cell test assemblies (see example in Ref. [15]) presumably because of differences in the flow fields (parallel vs. serpentine), which cause different mass transport losses.

The surface topologies and surface roughness of BPPs with different surface finishes and the GDL contact surface are shown in Fig. 5. Each map is a flow field land which contacts the GDL and is the interface for contact resistance. The rough finish typical of DMLS without polishing after the build (Fig. 5c) is characterized by numerous asperities with the occasional deeper pits (dark regions

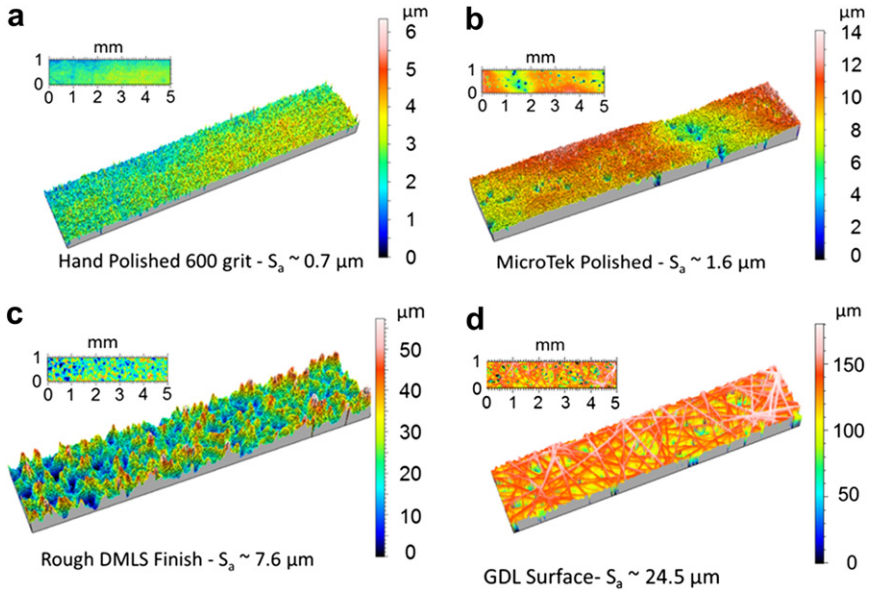

Fig. 5. Profilometry of BPP surface finishes and GDL surface: a) 600-grit polish, S_a ~ 0.7 µm, b) MicroTek polished, S_a ~ 1.6 µm, c) rough DMLS finish, S_a ~ 7.6 µm, d) surface of GDL contacting the BPP.

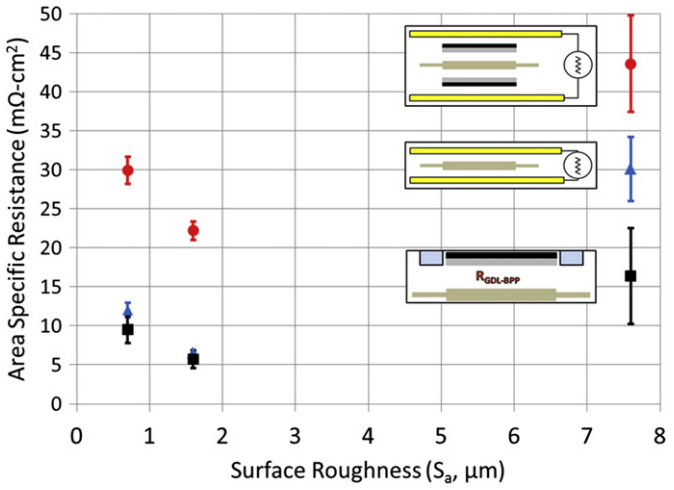

Fig. 6. Area-specific resistance vs. three different BPP surface roughnesses for three *ex situ* different cell configurations: (red circles) BPP between 2 GDLs; (blue triangles) BPP only; (black square) calculated contact resistance between the GDL and BPP. All measured at 1.00 ± 0.06 MPa reference stress area. (For interpretation of the references to color in this figure legend, the reader is referred to the web version of this article.)

in left of map) which are visible without magnification. The apparent surface roughness is consistent with parts manufactured by the successive melting of granules of metal powder, as in DMLS. The asperities can be as high as 20 μm and the surface has a roughness of 7.6 μm. Fig. 5a shows the lands after hand polishing with 600-grit sandpaper. Of the three finishes this is the smoothest with a surface showing a nearly uniform topology with a corresponding surface roughness of 0.7 μm. Fig. 5b shows the BPP land after MicroTek polishing. The surface is mostly smooth with some regions of waviness and remnants of the deeper pits (darks spots center of map) that were unable to be removed by the MicroTek process. The roughness after MicroTek polishing is 1.6 μm.

In accordance with the model presented by Y. Ein-Eli's group, it is expected that the DMLS rough finished would show significant interfacial contact resistance because of its numerous asperities

Table 1
Resistance of fuel cell components and interfaces, as measured herein and from the literature.

Component or interface	Symbol	(mΩ cm^2)[a]	Ref.
Measurement electrodes and circuit	$R_{Circuit}$	~0[b]	Experimental[c]
Graphitic carbon end plate	R_{Gr}	0.7	[29]
GDL	R_{GDL}	1.9[d]	[30]
BPP	R_{BPP}	0.005	[31]
CCM	R_{CCM}	13.6 ± 1	[27]
Electrodes to graphitic carbon end plate	R_{Au-Gr}	4.45 ± 0.20	Experimental
Graphitic carbon end plate to MPL	R_{Gr-MPL}	5.52 ± 0.50	Experimental
GDL to BPP	$R_{GDL-BPP}$	4.75 ± 1.55	Experimental
MPL to CCM	$R_{MPL-CCM}$	5.65 ± 0.81	Experimental

[a] Resistance values at 1.00 ± 0.06 MPa (145 ± 8 psi).
[b] Below accuracy of measurement device.
[c] Experimental values are a combination of measurement and calculation.
[d] Calculated using the conductivity of Toray® TGP-H-060.

with similar size to the fibrous contacting surface of the GDL [16]. Fig. 5d shows the fibrous contacting surface of the GDL, and it is clear from inspection than many of the peaks shown in the BPP in Fig. 5a–c would engage with voids in the fibrous surface. The interfacial contact resistance of the MicroTek and hand polished BPPs is less obvious. Fig. 6 shows the contact resistance at the BPP to GDL interface ($R_{BPP-GDL}$) and for comparison the contact resistance at the BPP to the Au electrode interface (R_{BPP-Au}) at a contact stress of 1.00 MPa. Both measurement sets are reported at area-specific contact resistance (mΩ cm^2) because this unit is the most commonly used in fuel cell evaluation. The familiar trend of contact resistance decreasing as the surface becomes smooth, but increasing as the surface becomes too smooth is observed and is in agreement with previous studies [16,17]. The absolute surface roughness at which the interfacial contact resistance increases (<1.7 μm) does not match the previous work exactly (<0.76 μm), but is very close considering the experimental differences between all three works, i.e., GDL, BPP material, and compressive stress. Three surface roughness explored in this work are not enough to determine an optimum BPP surface roughness for this GDLs, but is suggestive that one exists. Interestingly, the contact resistance between the BPP and a gold coated electrode shows a trend that mirrors the GDL interface resistance with slightly lower absolute

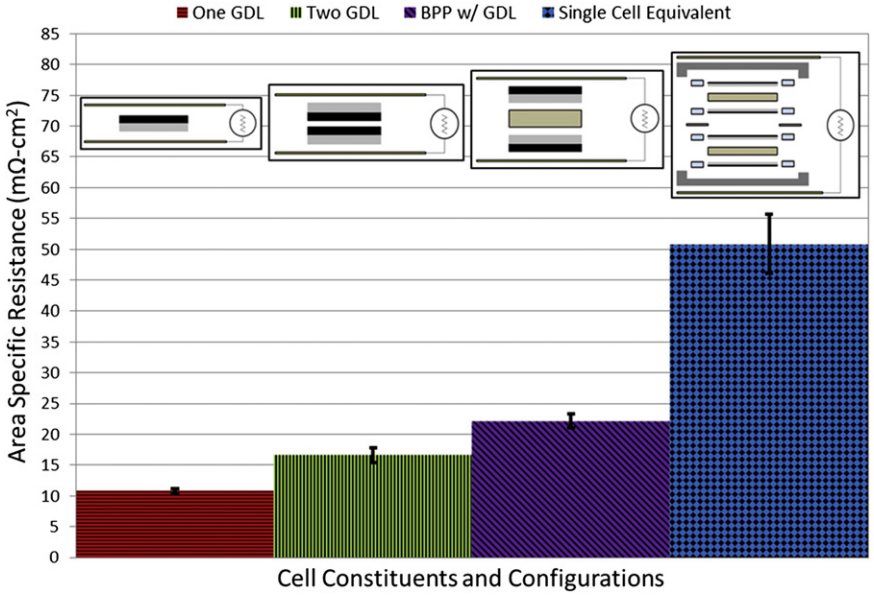

Fig. 7. Comparison of individual cell component and assembly resistances at reference area stress of 1.00 ± 0.06 MPa.

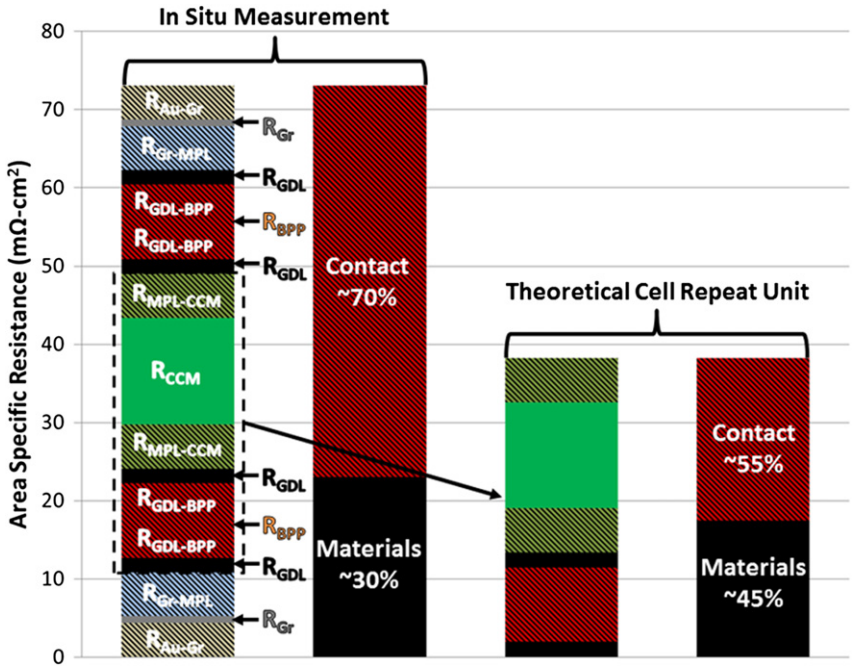

Fig. 8. Extrapolation of materials resistances (Table 1) and contact resistances from the test cell in this work (left) to the resistive contributions in a PEMFC (right).

values suggesting that this might be used as a screening technique for testing new surface treatments without involving GDL.

The through-plane resistance at 1.00 ± 0.06 MPa of selected *ex situ* configurations is summarized in Fig. 7. Qualitatively, they show the logical trend of increased resistance with an increase in the number of interfaces and components. The limitations of this reductionist approach are also apparent from the data. The through-plane resistance of one GDL is not equal to twice that of two GDLs stacked together because of the difference in the number of interfaces. The stack of two GDLs has three interfacial contact resistances not four. As a rough estimate, the through-plane resistance of a single GDL is 10 mΩ cm^2, which is in agreement with the GDL manufacturer's specifications [25].

Through the combination of systematic experiments and literature values it is possible to determine all of the resistance contributions of each component in the fuel cell. In order to link *ex situ* measurements to *in situ* measurements it is critical to get a good estimate of the CCM's bulk ionic resistance (R_{CCM}). For our estimates we use the work of K. R. Cooper on Nafion™ 212 (their Fig. 10) at 95% RH and 80 °C which has a conductivity of 110 mS cm^{-1} [27], which is consistent with ionomer conductivities recently reported by W. Liu [28]. A summary of bulk and contact resistances for all cell components is tabulated in Table 1. As expected the bulk resistance is negligible for the metal BPPs (R_{BPP}). The single largest contributor to the bulk resistance is associated with the R_{CCM}. The contact resistances between components, (e.g., $R_{GDL-BPP}$, $R_{MPL-CCM}$) were ~5 mΩ cm^2 regardless of the contact interfaces. TiO_2/Au coating is an effective way of reducing contact resistance and in these sets of experiments the BPP to GDL contact resistance is equivalent to a MPL to carbon contact resistance within experimental error. Note that the MPL to carbon interface lacks flow features and thus is not equivalent to a MPL carbon BPP interface, but is illustrative because it contains the appropriate materials.

Using the values in Table 1 it is possible to determine the contribution of interfacial resistances and the materials bulk resistance to total ohmic resistance. The contributions arising from the GDL, MPL, and CCM resistances and their associated interfacial resistances is shown in Fig. 8, with the measured values from our test cell on the left, and the extrapolated values for a unit cell on the right (comprised of: 1 BPP, 2 GDLs and 1 CCM). By such reduction of the data reported for our test cells, we surmise that for stacks using state-of-the-art CCMs the interfacial contact resistance between the CCMs and MPLs, and the GDLs and BPPs provide 55% of the resistance of each cell. With such advanced proton-exchange membranes with very high conductivity, contract resistances must be considered in their characterization and may even become more dominant at lower relative humidity [28]. Clearly, focus should be given to cell optimization to reduce contact resistances in full PEMFCs.

4. Conclusions

The major factor involved in PEMFC I^2R losses is in the interfacial contacts between different components. This contact resistance depends on many factors, ranging from BPP surface roughness and cell compression. A mechanical break-in procedure of cycling the compressive load decreases the area-specific resistance by 3 mΩ cm^2 at 1.00 ± 0.06 MPa (145 ± 8 psi). The GDL to BPP interfacial contact resistance has its lowest value of 4.75 mΩ cm^2 for gold/TiO_2-coated titanium BPP with a surface roughness of 1.6 μm at 1.00 MPa, but this is still one of the largest contributors to cell resistance. The use of enough compressive stress can remove some variable dependencies. The *ex situ* single-cell equivalent test showed that stress above 1.00 MPa eliminates GDL related resistance variation, and the *in situ* test showed that stress above 1.00 MPa eliminates temperature related resistance variation. This shifts the focus of ohmic resistance back to surface finish and interface dependencies.

When compared to state-of-the-art proton-exchange membranes resistances it was found that the CCM is the single largest contributor to the I^2R losses in the fuel cell, but overall contact resistances between the CCMs, MPLs, GDLs and BPPs dominate, contributing 55% of the cell resistance. Future research should focus on minimizing contact resistance between GDLs and other components through controlled surface finishes and novel coatings and further refinements to improve the contact stress distribution.

Acknowledgments

The authors would like to thank the Office of Naval Research for financial support of this work. NJN was a summer intern through the Naval Research Enterprise Intern Program (NREIP). We are grateful to Mr. Douglas Wheeler of DJW Technologies for his constructive advice and guidance.

References

[1] J. Larminie, A. Dicks, Fuel Cell Systems Explained, Second ed., Wiley and Sons, London, 2003.
[2] B. Smitha, S. Sridhar, A.A. Khan, J. Membr. Sci. 259 (2005) 10–26.
[3] T.R. Ralph, D.E. Barnwell, P.J. Bouwman, A.J. Hodgkinson, M.I. Petch, M. Pollington, J. Electrochem. Soc. 155 (2008) B411–B422.
[4] B. Cunningham, D.G. Baird, J. Mater. Chem. 16 (2006) 4385–4388.
[5] P. Trogadas, J. Parrondo, V. Ramani, Electrochem. Solid-State Lett. 11 (2008) B113–B116.
[6] P.J. Hamilton, B.G. Pollet, Fuel Cells 10 (2010) 489–509.
[7] H. Wang, M.A. Sweikart, J.A. Turner, J. Power Sources 115 (2003) 243–251.
[8] J.S. Kim, W.H.A. Peelen, K. Hemmer, R.C. Makkus, Corros. Sci. 44 (2002) 635–655.
[9] I. Betova, M. Bojinov, A. Englund, G. Fabricius, T. Laitinen, K. Makela, T. Saario, G. Sundholm, Electrochim. Acta 46 (2001) 3627–3640.
[10] D.P. Davies, P.L. Adcock, M. Turpin, S.J. Rowen, J. Appl. Electrochem. 30 (2000) 101–105.
[11] E.C. Santos, M. Shiomi, K. Osakada, T. Laoui, Int. J. Mach. Tools Manuf. 46 (2006) 1459–1468.
[12] M.W. Khaing, J.Y.H. Fuh, L. Lu, J. Mater. Process. Tech. 113 (2001) 269–272.
[13] L. Zhang, J. Finch, G. Gontarz, C. Wang, ECS Trans. 33 (2010) 955–961.
[14] P. Zhou, C.W. Wu, G.J. Ma, J. Power Sources 163 (2007) 874–881.
[15] B.D. Gould, O.A. Baturina, K. Swider-Lyons. 188 (2009) 89–95.
[16] A. Kraytsberg, M. Auinat, Y. Ein-Eli, J. Power Sources 164 (2007) 667–703.
[17] B. Avasarala, P. Haldar, J. Power Sources 188 (2009) 225–229.
[18] P. Zhou, C.W. Wu, G.J. Ma, J. Power Sources 159 (2006) 1115–1122.
[19] J. Ihonen, F. Jaouen, G. Lindbergh, G. Sundholm, Electrochim. Acta 46 (2001) 2899–2911.
[20] US Fuel Cell Council, Electrical Conductivity Testing Protocol (2009).http://www.usfcc.com/resources/technicalproducts.html#form.
[21] X. Wang, Y. Song, B. Zhang, J. Power Sources 179 (2008) 305–309.
[22] C.-Y. Wen, Y.-S. Lin, C.-H. Lu. 192 (2009) 475–485.
[23] http://www.microtekfinishing.com/binc_mmp.php.
[24] Y. Zhou, G. Lin, A.J. Shih, S.J. Hu, J. Power Sources 163 (2007) 777–783.
[25] http://www.sglgroup.com/export/sites/sglcarbon/_common/downloads/products/product-groups/su/fuel-cell-components/GDL_24_25_Series_Gas_Diffusion_Layer.pdf.
[26] T.J. Mason, J. Millichamp, T.P. Neville, A. El-kharouf, B.G. Pollet, J. Power Sources 219 (2012) 52–59.
[27] K.R. Cooper, J. Electrochem. Soc. 157 (2010) B1731–B1739.
[28] W. Liu, T. Suzuki, H. Mao, T. Schmiedel, ECS Trans. 50 (2012) 51–64.
[29] H.O. Pierson, Handbook of Carbon, Graphite, Diamond and Fullerenes (1993) (New Jersey).
[30] http://www.torayca.com/en/index.html.
[31] http://asm.matweb.com/search/SpecificMaterial.asp?bassnum=MTP641.